Supporting Information

Zirconia-Supported ZnO Single Layer for Syngas Conversion Revealed from Machine-Learning Atomic Simulation

Siyue Chen, Sicong Ma and Zhi-Pan Liu*

Email: zpliu@fudan.edu.cn

Collaborative Innovation Center of Chemistry for Energy Material, Shanghai Key Laboratory of Molecular Catalysis and Innovative Materials, Key Laboratory of Computational Physical Science, Department of Chemistry, Fudan University, Shanghai 200433, China

Table of Contents

Method 2
Stochastic surface walking global exploration with neural network potential (SSW-NN) 2
Global dataset generation 3
Global NN PES fitting 5
Gibbs free energy correction 6
Methanol production rate 6
Bulk phase exploration of GMs 7
Solid-solution phase structures 8
Surface structures for Zn-O on ZrO_2 9
Oxygen vacancy generation 10
Adsorption sites conversion for CO/H_2 11
Microkinetics simulation 12
Bader charge analysis 13
PDOS of O_{3c} on Zn-O/M(001) 14
Wave Function of ZnO(1010) surface 15
Optimized XYZ position for Zn-O/M(001) surface 16
Optimized XYZ position for ZnO($11\bar{2}0$)/M(100) surface 19
References 22

Method

SSW-NN method. SSW-NN method is utilized to perform a comprehensive exploration on the phase space of ternary ZnZrO system, which combines the global neural network (G-NN) potential[1–3] with stochastic surface walking (SSW) method[4–7] for fast and accurate global PES exploration as implemented in LASP code.[8] G-NN potential was trained based on global PES data sets generated by plane-wave density functional theory (DFT) calculations SSW global search trajectories. The ZnZrO G-NN potential was iteratively improved by self-learning until the deviation with DFT energy and force to 3.53 meV/atom and 0.12 eV/Å. With the G-NN potential, a vast number of minima (>10^7) were searched at different Zn:Zr ratios, for both bulk and surfaces. The low energy structures were verified by DFT calculations, from which the global minima was determined (also see **SI** for dataset and benchmarking details).

DFT calculation. All DFT calculations were performed using the plane wave method with projector-augmented wave (PAW) pseudopotentials implemented in VASP. [9,10] The DFT functional utilized is GGA-PBE.[11] The kinetic energy cutoff was set as 450 eV. An automatic Monkhorst-Pack scheme for k-mesh was utilized which adopt the mesh with 25- and 15-times reciprocal lattice vectors for bulk and surface calculations, respectively. For convergence of geometry, the maximum force on coordinate was set as 0.05eV/Å for force. For van der Waals correction, zero damping DFT-D3 method of Grimme was adopted for Gibbs free energy profile and microkinetics simulation.[12,13]

Free energy correction and Microkinetics. The Gibbs free energy correction was performed to obtain the syngas conversion reaction profile at the typical reaction conditions (673 K, 3 Mpa, H_2:CO=2:1), where the zero-point energy of states and the entropy contributions to gas phase molecules are taken into account. Microkinetics simulation was performed to evaluate the theoretical TOF and to identify the apparent activation energy. In the simulation, the pressure of CO and H_2 were fixed to simulate a fluidized-bed catalytic reactor during the whole process. The total time is set to 1E-3 second and the temperature ranges from 535 K to 723 K. Detailed of evaluation from TOF to production rate is listed in the following sections.

Stochastic surface walking global exploration with neural network potential (SSW-NN)

The SSW-NN method is applied to sample the global potential energy surfaces of $Zn_xZr_yO_z$ system with varied Zn:Zr ratios. While traditional DFT calculations are frustrated for the global optimization of complex systems due to the too-high computational cost, SSW-NN method provides a general solution for PES scanning with both high efficiency and high accuracy. More specifically, SSW method is utilized to explore PES and locate global/local minima, whereas NN potential is trained based on DFT dataset and delivers a high speed of PES evaluation, 3~4 orders of magnitude faster than DFT. The application of SSW-NN method can be divided into five steps: (1) Generating the global dataset from the SSW global optimization trajectories and computing the dataset using DFT calculations; (2) Training the NN potential with dataset; (3) Benchmarking the accuracy between the current NN potential and DFT calculation for selected structures from SSW trajectories and retraining the NN potential by adding new dataset; (4) iteratively performing (1-3) steps until the PES deviation is low enough (typically below 10 meV/atom); (5) Performing the SSW global optimization on the NN PES for target problem.

Global dataset generation

The global dataset is built iteratively during the self-learning of NN potential. The initial data of the global dataset comes from the DFT-based SSW simulation and all the other data is taken from NN-based SSW PES exploration. SSW simulations were run in parallel with many different compositions (at different Zn:Zr ratio), different morphologies, including bulk, layer and clusters, compositions and different atom numbers per unit cell (10 ~ 160). These SSW simulations generate more than 10^7 structures on PES and 27,101 structures were selected as the final global dataset that is computed by high accuracy DFT calculations. The final dataset is described in **Table S1**.

Table S1. Structure information of global dataset. Listed data are the number of the structures in the global dataset, as distinguished by the chemical formula, the number of atoms (N), the type of structures (cluster, bulk, layer).

Species	atoms	cluster	layer	bulk	total
O1-Zn12	13	0	575	0	575
O2-Zr8	10	0	29	72	101
O2-Zr10	12	0	311	0	311
O2-Zn17	19	0	7	183	190
O3-Zr18	21	0	77	31	108
O4-Zr4	8	0	40	204	244
O4-Zr8	12	0	26	132	158
O4-Zr22	26	0	8	32	40
O4-Zn15	19	0	0	21	21
O5-Zr27	32	0	1	29	30
O6-Zr4	10	0	0	13	13
O6-Zr8	14	0	30	149	179
O6-Zr15	21	0	69	0	69
O6-Zr18	24	0	6	36	42
O6-Zn5-Zr1	12	0	8	21	29
O6-Zn6	12	1119	0	0	1119
O6-Zn8	14	0	15	218	233
O7-Zn4-Zr2	13	0	3	56	59
O7-Zn5-Zr1	13	0	9	69	78
O7-Zn8	15	0	18	218	236
O7-Zn16	23	0	0	25	25
O8-Zr4	12	0	60	4591	4651
O8-Zr8	16	0	32	135	167
O8-Zn1-Zr4	13	0	8	15	23
O8-Zn2-Zr3	13	0	3	8	11
O8-Zn3-Zr3	14	0	94	78	172
O8-Zn4-Zr2	14	0	32	88	120
O8-Zn5-Zr1	14	0	29	98	127
O8-Zn8	16	292	12	3851	4155
O9-Zn3-Zr3	15	0	197	443	640

O18-Zr8	18	0	56	174	230
O10-Zr22	32	0	0	27	27
O10-Zn10	20	0	1097	82	1179
O10-Zn16	26	0	1	55	56
O10-Zn24	34	0	12	249	261
O11-Zn15	26	0	0	22	22
O11-Zn16	27	0	26	0	26
O12-Zr8	20	0	0	149	149
O13-Zn15	28	0	134	40	174
O14-Zr8	22	0	0	62	62
O14-Zn10-Zr2	26	0	9	374	383
O14-Zn15	29	0	0	39	39
O14-Zn16	30	0	144	39	183
O15-Zr9	24	0	0	105	105
O15-Zn8-Zr4	27	0	5	182	187
O16-Zr8	24	9	8	89	97
O16-Zn6-Zr5	27	0	1	3	4
O16-Zn6-Zr6	28	0	70	151	221
O16-Zn7-Zr5	28	0	1	23	24
O16-Zn8-Zr4	28	0	11	437	448
O16-Zn9-Zr3	28	0	2	8	10
O16-Zn14	30	0	288	10	298
O16-Zn16	32	0	312	108	420
O17-Zn2-Zr8	27	0	10	443	453
O17-Zn6-Zr6	29	0	47	561	608
O18-Zr12	30	0	120	6	126
O18-Zn2-Zr8	28	0	5	462	467
O18-Zn5-Zr6	29	0	72	84	156
O18-Zn6-Zr6	30	0	49	542	591
O22-Zn8-Zr8	38	0	0	152	152
O23-Zn6-Zr9	38	0	71	1	72
O23-Zn8-Zr8	39	0	41	116	157
O24-Zn6-Zr9	39	0	54	1	55
O24-Zn7-Zr8	39	0	39	137	176
O24-Zn7-Zr9	40	0	83	0	83
O24-Zn8-Zr7	39	0	52	154	206
O24-Zn8-Zr8	40	0	167	165	332
O32-Zn1-Zr16	49	0	21	6	27
O38-Zn10-Zr15	63	0	73	0	73
O39-Zn10-Zr15	64	0	65	0	65
O40-Zn10-Zr15	65	0	76	0	76
O40-Zn11-Zr15	66	0	69	0	69
O79-Zn16-Zr32	127	0	50	0	50
O80-Zn16-Zr32	128	0	39	0	39

O95-Zn32-Zr32	159	0	22	0	22
O96-Zn32-Zr32	160	0	10	0	10
total	--	2266	5338	19497	27101

Global NN PES fitting

The global NN potential is generated using the method as introduced in our previous work.[1,2] To pursue a high accuracy for PES, we have adopted a large set of power-type structure descriptors (PTSDs), which contains 324 descriptors for every element with only power-type structure descriptors, including 132 two-body, 146 three-body, 22 four-body descriptors, and compatibly, the network utilized is also large involving three-hidden layers (324-80-60-60-1 net). Min-max scaling is utilized to normalization the training data sets. Hyperbolic tangent function is used to activate the hidden layers, while a linear transformation is applied to the output layer of all networks. The limited-memory Broyden-Fletcher-Goldfarb-Shanno (L-BFGS) method is used to minimize the loss function to match DFT energy, force and stress. The final energy and force criterions of the root mean square (RMS) errors are around 3.53 meV/atom and 0.120 eV/Å respectively. To benchmark the accuracy of NN PES, we select 26 ZnZrO crystal structures to compare the NN results with the DFT calculation results. It has an average energy error of 1.876 meV/atom, which is quite standard for NN potentials and accurate enough for searching the stable structure candidates. The details for the comparison between DFT and NN results can be found in **Table S2**.

Table S2. Benchmark of NN calculations for ZnZrO systems as compared with DFT results. Listed data include the compositions, total atom number (N_{atom}), DFT energy, NN energy and energy differences between DFT energy and NN energy (E_{diff}, meV/atom), covering both bulk and surface structures.

composition	N_{atom}	DFT energy (eV)	NN energy (eV)	E_{diff} (meV/atom)
Zn_2O_2	4	-17.856	-17.857	-0.608
(m-)Zr_4O_8	12	-114.246	-114.254	-0.667
$Zn_4Zr_{124}O_{252}$	380	-3576.046	-3575.901	0.381
$Zn_1Zr_{31}O_{63}$	95	-892.827	-893.235	-4.294
$Zn_4Zr_{96}O_{196}$	296	-2774.461	-2774.579	-0.399
$Zn_1Zr_{24}O_{49}$	74	-683.105	-683.108	-0.041
$Zn_4Zr_{60}O_{124}$	188	-1748.025	-1747.858	0.886
$Zn_1Zr_{15}O_{31}$	47	-435.846	-436.120	-5.830
$Zn_4Zr_{44}O_{92}$	160	-1291.036	-1290.855	1.129
$Zn_1Zr_{11}O_{23}$	35	-321.639	-322.043	-11.539
$Zn_4Zr_{28}O_{60}$	92	-834.063	-833.862	2.184
$Zn_1Zr_7O_{15}$	23	-207.880	-207.992	-4.8713
$Zn_8Zr_{32}O_{72}$	112	-983.273	-983.293	0.178
$Zn_1Zr_4O_9$	14	-122.482	-122.541	-4.184
$Zn_8Zr_{24}O_{56}$	88	-753.719	-753.665	0.610
$Zn_1Zr_3O_7$	11	-93.897	-93.960	-5.761
$Zn_8Zr_{16}O_{40}$	64	-526.644	-526.390	3.976
$Zn_1Zr_2O_5$	8	-65.006	-65.125	-14.875

$Zn_{16}Zn_{24}O_{64}$	104	-824.776	-824.976	-1.920
$Zn_8Zr_8O_{24}$	40	-298.470	-298.560	-2.275
$Zn_{12}Zr_8O_{28}$	48	-333.514	-333.464	1.055
$Zn_{14}Zr_6O_{26}$	46	-293.536	-293.545	-0.198
$Zn_{16}Zr_4O_{24}$	44	-255.321	-255.505	-4.185
$Zn_7Zr_1O_9$	17	-90.104	-90.080	1.385
$Zn_{18}Zr_2O_{22}$	42	-215.823	-215.786	0.886
$Zn_{23}Zr_1O_{25}$	49	-232.281	-232.320	-0.788
$Zn_4Zr_{32}O_{68}$ | M(001)	104	-945.344	-945.301	-0.417
$Zn_4Zr_{32}O_{68}$ | M(011)	104	-942.829	-942.916	0.832
$Zn_4Zr_{32}O_{68}$ | M(100)	104	-945.056	-944.740	-3.045
$Zn_8Zr_{32}O_{72}$ | M(111)	112	-976.291	-976.227	-0.569
$Zn_8Zr_{32}O_{72}$ | M($\bar{1}$11)	112	-978.247	-977.950	-2.651
$Zn_8Zr_{32}O_{72}$ | T(001)	112	-973.007	-972.864	-1.277
$Zn_4Zr_{32}O_{68}$ | T(100)	104	-940.313	-939.962	-3.380
$Zn_8Zr_{32}O_{72}$ | T(101)	112	-973.831	-973.612	-1.952
$Zn_4Zr_{32}O_{68}$ | T(111)	104	-941.080	940.723	-3.432

* Mean error between DFT energy and NN energy is 1.876 meV/atom.

Gibbs free energy correction

The Gibbs free energy G[X] of bulks/surfaces can be approximated by their DFT total energy E[X] with the appropriate inclusion of zero-point-energy (ZPE) since it is known that the vibration entropy and the PV term contributions of solid phases are negligibly small. The chemical potential μ for gas phase molecules μ[X] can be calculated as follows:

$$\mu[X](p, T) = E[X] + ZPE[X] + [H[X](p^0, T) - H[X](p^0, 0K) - TS[X](p^0, T) + k_BT \ln p/p^0]$$

where enthalpy (H) and entropy (S) terms of gas phase molecules are taken from the standard thermodynamics data.

Methanol production rate

Our calculated methanol generation rate is 7.38 s^{-1} at 673 K and 3 MPa syngas (H_2:CO = 2:1). The methanol yield is required to be evaluated in logarithm of mmol g^{-1} h^{-1} to compare with experiment.[14] In experiment, the surface area of ZnZrO catalysts with Zn:Zr = 1:16 is 62 m^2/g. From our theoretical calculation, the surface area of one exclusive Zn active site on Zn-O/M(001) is 1.09E-18 m^2 and The TOF of Zn-O/M(001) is 7.384 s^{-1} (vdW-corrected) from microkinetics simulation.

Assumption 1: All Zn content engages into the formation of Zn-O/M(001), which takes up 1/17 of the total surface area of ZnZrO (62 *1/17 m^2/g).

Assumption 2: The effective active sites are assumed no more than 2%.

The number of effective active site is then calculated to be 3.35E+18 * 0.02=6.69E+16 site/g.

The logarithm of methanol production rate is evaluated as following:

ln(6.69E+16 * 7.384 s^{-1} * 3600 / (6.02E+23) * 1000 mmol) = 1.08 mmol g^{-1} h^{-1}

Bulk phase exploration of GMs

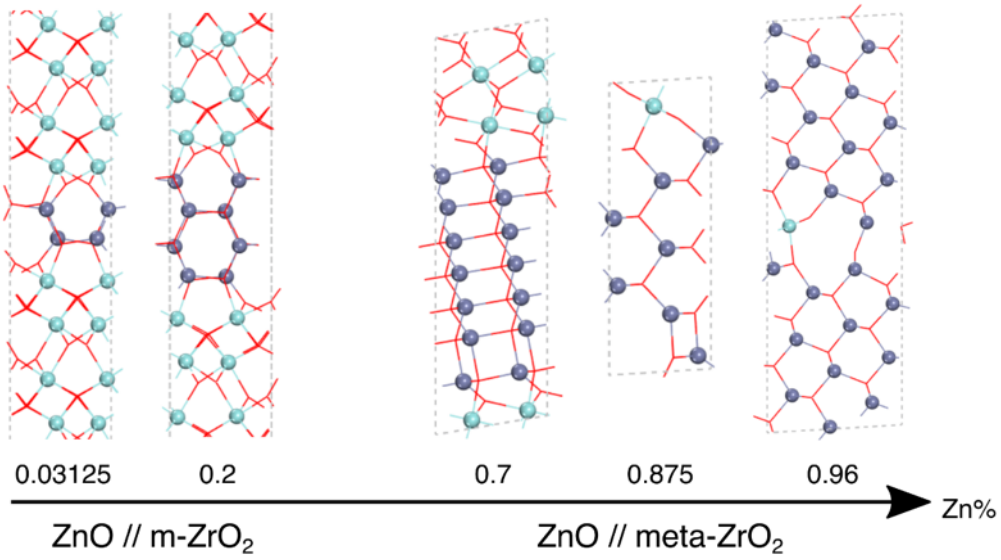

Figure S1. The structures of identified global minima of ZnZrO with varied Zn contents.

Table S3. The formation energies of identified global minima for ZnZrO with varied Zn contents.

Composition	Zn content (%)	$E_{f,\ bulk}$ (eV)
$Zn_4Zr_{124}O_{252}$	3.13	0.0051
$Zn_4Zr_{96}O_{196}$	4.00	0.0160
$Zn_4Zr_{60}O_{124}$	6.25	0.0111
$Zn_4Zr_{44}O_{92}$	8.33	0.0150
$Zn_4Zr_{28}O_{60}$	12.5	0.0228
$Zn_8Zr_{32}O_{72}$	20.0	0.0294
$Zn_8Zr_{24}O_{56}$	25.0	0.0568
$Zn_8Zr_{16}O_{40}$	33.3	0.0441
$Zn_{16}Zn_{24}O_{64}$	40.0	0.0554
$Zn_8Zr_8O_{24}$	50.0	0.0602
$Zn_{12}Zr_8O_{28}$	60.0	0.0755
$Zn_{14}Zr_6O_{26}$	70.0	0.1087
$Zn_{16}Zr_4O_{24}$	80.0	0.0739
$Zn_7Zr_1O_9$	87.5	0.1060
$Zn_{18}Zr_2O_{22}$	90.0	0.0912
$Zn_{23}Zr_1O_{25}$	96.0	0.0651

Solid-solution phase structures

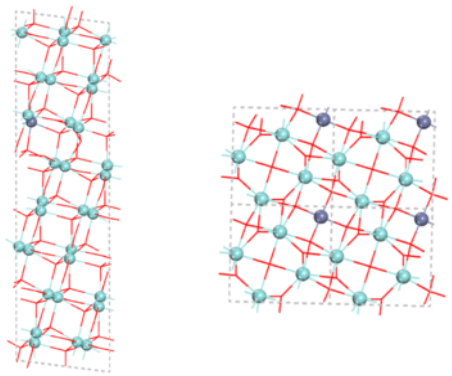

Figure S2. The structures of metastable solid-solution phases identified from SSW-NN. Left: $Zn_1Zr_{31}O_{73;}$ Right: $Zn_1Zr_4O_9$ (see Table S4)

Table S4. The formation energies of solid-solution phases

Composition	Zn content (%)	$E_{f,\ bulk}$ (eV per O atom)	Bulk matrix
$Zn_1Zr_{31}O_{73}$	3.13	0.0239	m-ZrO_2
$Zn_1Zr_4O_9$	20.0	0.0769	t-ZrO_2

Surface structures for Zn-O on ZrO_2

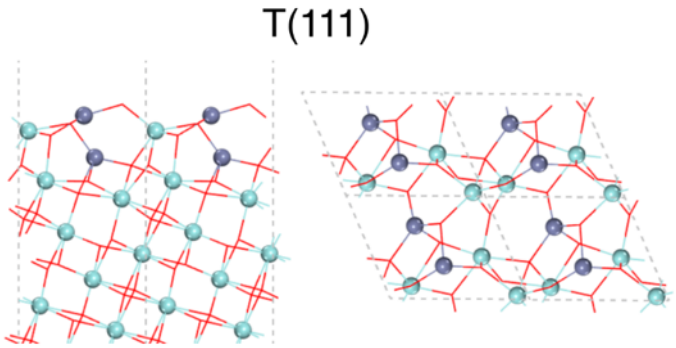

Figure S3. The structure of Zn-O overlayers on t-ZrO_2(111) surface. Left: side view; Right: top view.

Table S5. Energetics for ZnO overlayers on nine low-Miller-index ZrO_2 surfaces. Listed data include the concentration of surface Zn-O (Zn-O/A_{surf}), the formation energy ($E_{f,\ surf}$), and the surface energy ($\gamma_{\_ZnZrO}$).

Surface	Zn-O/A_{Surf} (mmol/m^2)	$E_{f,\ surf}$ (eV)	$\gamma_{\_ZnZrO}$ (J/m^2)
M(001)	0.440	-0.111	1.271
M(100)	0.427	-0.139	1.314
M(111)	0.434	+0.233	-
M($\bar{1}$11)	0.479	+0.215	-
M(011)	0.304	+0.149	-
T(101)	0.521	+0.207	-
T(111)	0.369	-0.032	1.114
T(100)	0.317	+0.017	-
T(001)	0.457	+0.086	-

Oxygen vacancy generation

Table S6. The oxygen vacancy formation energies (E_{OV}) on surfaces*

Surface	O_v type	E_{OV} (eV)
Zn-O/M(001)	0.25ML $O_{3c,\ surf}$	3.366
Zn-O/M(001)	0.5ML $O_{3c,\ surf}$ + $O_{4c,\ surf}$	4.357
ZnO($10\bar{1}0$)	0.25ML O_{surf}	2.879
ZnO($11\bar{2}0$)	0.25ML O_{surf}	2.725

* E_{OV} is computed with respect to half of DFT energy of O_2.

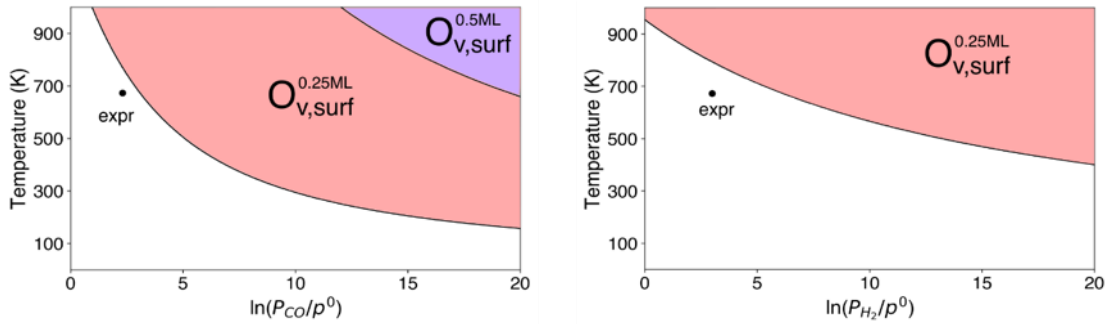

Figure S4. Thermodynamic phase diagram of oxygen vacancy (O_V) concentrations for Zn-O/M(001) surface in contact with CO and H_2 under syngas conversion conditions. These two phase diagram of O_v are computed based on Gibbs free energy data for the reaction ($Zn_xZr_yO_z$ + nCO → $Zn_xZr_yO_{z-n}$+ nCO_2) and ($Zn_xZr_yO_z$ + nH_2 → $Zn_xZr_yO_{z-n}$+ nH_2O) from DFT calculations. The typical experiment condition (673K, 3Mpa, H_2:CO=2:1) is labeled as "expr" in the figure. For CO-assisted O_v generation, the equilibrium pressure of CO_2 is evaluated at 673 K, 0.135 Mpa, according to the experimental results (CO conversation at ~30% and CO_2 selectivity at ~45%).[14] For H_2-assisted O_v generation, the pressure of H_2O is set to 0.01 Kpa according to experiment.[14]

Adsorption sites for CO/H_2 on Zn-O/M(001)

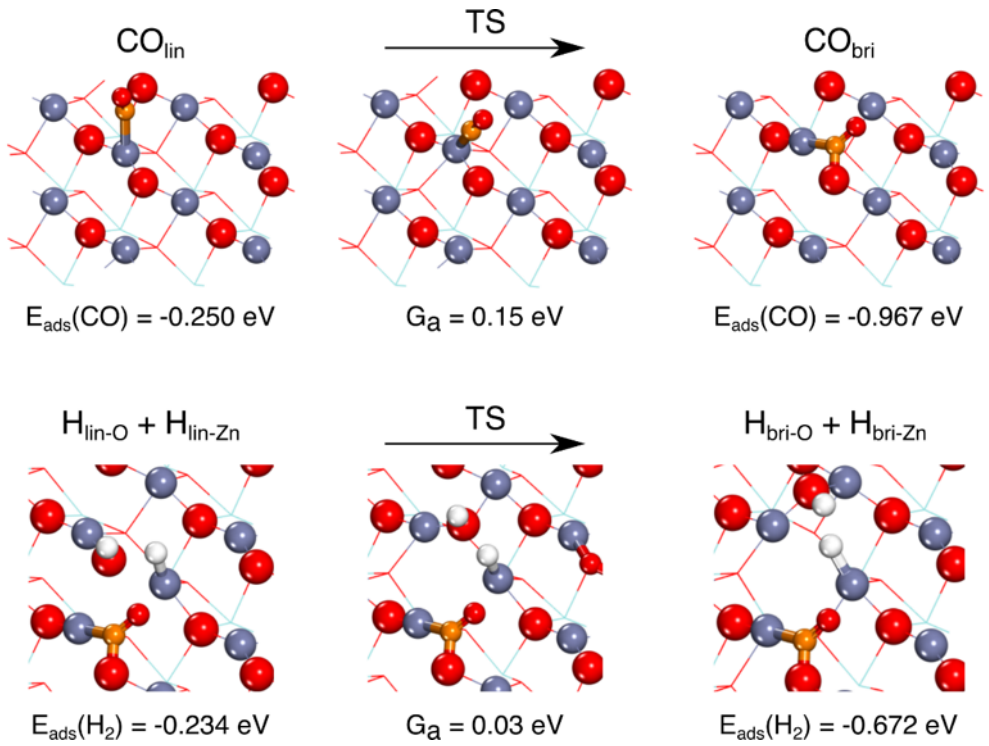

Figure S5 The conversion between different adsorbed configurations for H and CO on Zn-O/M(001). The first row illustrates the conversion for adsorbed CO from the atop site adsorption to the bridging configuration (including IS, TS, FS), named as CO_{lin} and CO_{bri}. Similarly, The second row illustrates the conversion of adsorbed H on Zn-O/M(001). Only stable sites of CO/H_2 (CO_{bri}, H_{bri-o} and H_{bri-Zn}) are presented in **Fig. 2a**.

Microkinetics simulation

Table S7. The syngas conversion reaction energy, ZPE corrections, Van der Waals (vdW) correction and Gibbs free energy barriers (forward and reverse) for all elementary steps (673 K). The reaction step (1 to 8) can be found in note*

Step	$\triangle E_{FS-IS}$	$\triangle E_{TS-IS}$	$\triangle ZPE_{FS-IS}$	$\triangle ZPE_{TS-IS}$	$G_{a,+}$	$G_{a,-}$	$\triangle VDW_{FS-IS}$	$\triangle VDW_{TS-IS}$	$G_{a,+}^{VDW}$	$G_{a,-}^{VDW}$
1	-0.250	1.240	0.031	0	1.240	0.216	-0.140	0	1.240	0.359
2	-0.717	0.138	0.074	0.017	0.155	0.798	-0.025	-0.023	0.132	0.800
3	-0.235	0.697	0.185	0	0.697	0.049	-0.129	0	0.697	0.178
4	-0.438	0.036	0.017	-0.001	0.035	0.456	0.037	0.019	0.054	0.438
5	0.314	0.964	0.059	-0.087	0.877	0.504	0.009	-0.005	0.872	0.490
6	0.289	1.014	-0.011	-0.141	0.873	0.595	-0.005	-0.041	0.832	0.559
7	-0.850	0.365	0.156	0.005	0.370	1.064	0.042	-0.064	0.306	0.958
8	-1.130	0.780	-0.043	-0.043	0.737	1.910	0.237	0.204	0.942	1.878

*

1	$CO_{(g)} + \# \rightarrow CO_{lin}^{\#}$
2	$CO_{lin}^{\#} + * \rightarrow CO_{bri}^{\#*}$
3	$H_{2(g)} + * + \# \rightarrow H_{lin}^{\#} + H_{lin}^{*}$
4	$H_{lin}^{\#} + H_{lin}^{*} \rightarrow H_{bri}^{\#} + H_{bri}^{*}$
5	$CO_{bri}^{\#*} + H_{bri}^{\#} \rightarrow CHO^{\#\#} + *$
6	$CHO^{\#\#} + H_{bri}^{*} \rightarrow CH_2O^{\#} + \# + *$
7	$CH_2O^{\#} + H_{bri}^{\#} \rightarrow CH_3O^{\#\#}$
8	$CH_3O^{\#\#} + H_{bri}^{*} \rightarrow CH_3OH(g) + * + 2\#$

In the steps, * denotes the surface O adsorption site, # denotes the surface Zn adsorption site. For the adsorption of CO/H_2, $\triangle G_{gas}$ (1.240 eV for CO and 0.697 eV for H_2 under 673 K and 3 Mpa, H_2:CO = 2:1) describes the loss of entropy in adsorption, defined as $G_{a,+}$. For the desorption of CH_3OH, $\triangle G_{gas}$ is -1.98 eV with the gas CH_3OH under 673K and 0.0 1Kpa.

Table S8. Volumes of chemical species at the equilibrium of kinetics simulation.*

Species	$CO_{(g)}$	$H_{2(g)}$	$CO_{bri}^{\#*}$	H_{bri}^{*},$H_{bri}^{\#}$	$CHO^{\#\#}$	$CH_2O^{\#}$	$CH_3O^{\#\#}$	*	#	$CH_3OH_{(g)}$
Volume (0 s)	10	20	0	0	0	0	0	1	1	0
Volume (1E-3 s)	10	20	1.38E-2	2.31E-1	4.39E-6	1.92E-9	2.59E-5	0.75	0.73	1.75E-2

* The pressure of CO and H_2 are fixed to simulate a fluidized-bed catalytic reactor during the whole process.

Table S9. TOFs (with vdW correction) of syngas conversion reaction at different temperatures.

Temperature (K)	TOF (s^{-1})
523	1.333
550	3.793
573	6.928
600	9.361
623	9.937
673	7.384
723	3.953

Bader charge analysis

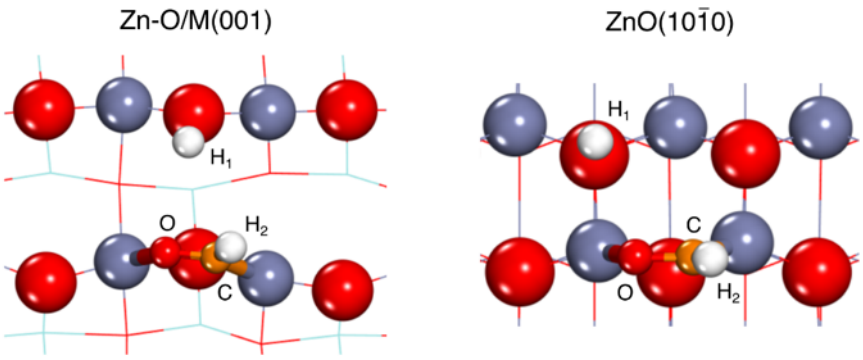

Figure S6. The adsorption configuration of CHO and H groups on Zn-O/M(001) and ZnO (10-10) surfaces.

Table S10. The electron transfer of CHO and H adsorbate on Zn-O/M(001) and ZnO (10-10) surfaces based on Bader charge analysis.

surface	Atom	$\Delta e^-_{(bader\text{-}initial)}$	Δe^-_{tot}
Zn-O/M(001)	C	-0.549	
	O	+1.067	0.46
	H_2	-0.058	
	H_1	-0.631	-0.63
ZnO (10-10)	C	-0.487	
	O	+1.047	0.47
	H_2	-0.093	
	H_1	-0.587	-0.59

PDOS of O_{3c} on Zn-O/M(001)

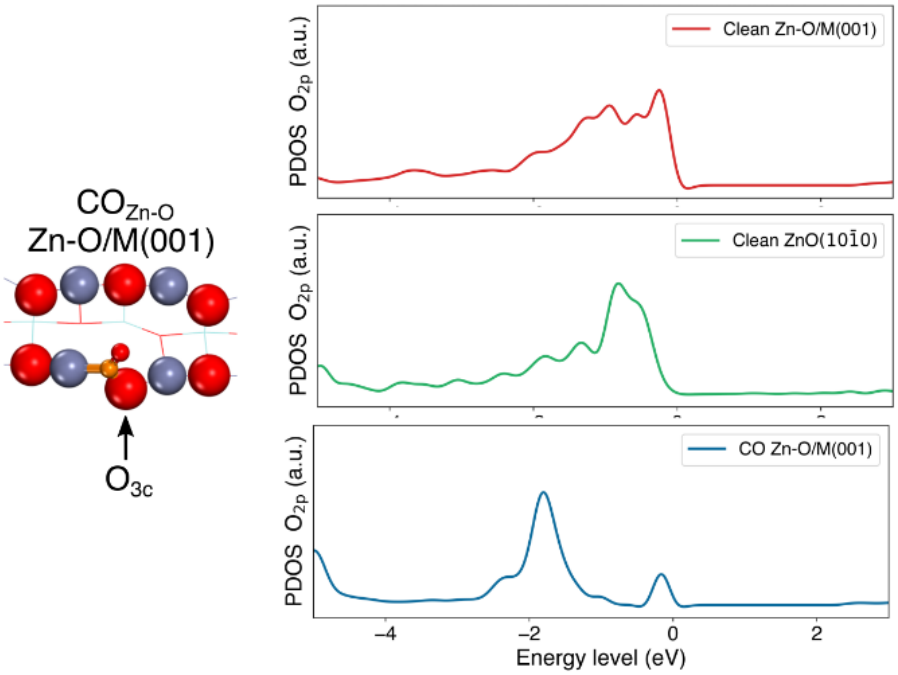

Figure S7. PDOS of O 2p orbital on Zn-O/M(001), ZnO(10$\bar{1}$0) and the CO-adsorbed Zn-O/M(001) surfaces.

Wave Function of $ZnO(10\bar{1}0)$ surface

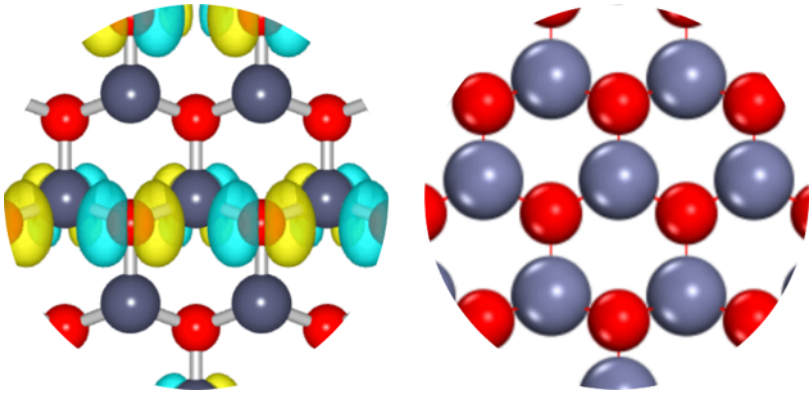

Figure S8. Wavefunction contour plot of VBM for clean $ZnO(10\bar{1}0)$ surface (left) and its atomic structure (right). The 3D isosurface value is set as 0.002 e $Å^{-3}$.

Optimized XYZ position for Zn-O/M(001) surface

Zn-O/M(001)
1.0

10.3746004105	0.0000000000	0.0000000000
0.0000000000	10.5298004150	0.0000000000
0.0000000000	0.0000000000	25.0000000000

O	Zr	Zn
72	32	8

Cartesian

4.212398997	1.008017786	6.636250019
4.212398997	6.272918072	6.636250019
9.399699202	1.008017786	6.636250019
9.399699202	6.272918072	6.636250019
1.347349329	3.582553870	7.124999911
1.347349329	8.847454077	7.124999911
6.534649535	3.582553870	7.124999911
6.534649535	8.847454077	7.124999911
1.763163272	0.963792660	8.333499730
1.763163272	6.228693103	8.333499730
6.950463632	0.963792660	8.333499730
6.950463632	6.228693103	8.333499730
3.730706386	3.906977005	8.845499903
3.730706386	9.171877213	8.845499903
8.918006591	3.906977005	8.845499903
8.918006591	9.171877213	8.845499903
4.194554568	1.356238343	9.204500169
4.194554568	6.621138237	9.204500169
9.381854773	1.356238343	9.204500169
9.381854773	6.621138237	9.204500169
0.837541477	4.409038103	9.941499680
0.837541477	9.673938310	9.941499680
6.024841914	4.409038103	9.941499680
6.024841914	9.673938310	9.941499680
1.410011987	1.776587999	10.905499756
1.410011987	7.041488207	10.905499756
6.597311883	1.776587999	10.905499756
6.597311883	7.041488207	10.905499756
3.240195138	3.988688447	11.642500013
3.240195138	9.253588341	11.642500013
8.427495343	3.988688447	11.642500013
8.427495343	9.253588341	11.642500013
3.745126876	1.276211839	11.842750013
3.745126876	6.541112282	11.842750013

8.932427081	1.276211839	11.842750013
8.932427081	6.541112282	11.842750013
0.388010053	3.488312208	12.579749525
0.388010053	8.753212416	12.579749525
5.575310336	3.488312208	12.579749525
5.575310336	8.753212416	12.579749525
0.908711266	0.946944929	13.646249473
0.908711266	6.211845137	13.646249473
6.096011239	0.946944929	13.646249473
6.096011239	6.211845137	13.646249473
2.820438904	3.922771816	14.274750650
2.820438904	9.187672024	14.274750650
8.007739109	3.922771816	14.274750650
8.007739109	9.187672024	14.274750650
3.280863765	1.355501198	14.547500014
3.280863765	6.620401405	14.547500014
8.468163970	1.355501198	14.547500014
8.468163970	6.620401405	14.547500014
0.056645320	4.249090379	15.173999965
0.056645320	9.513990586	15.173999965
5.243945771	4.249090379	15.173999965
5.243945771	9.513990586	15.173999965
0.198362363	1.388564797	16.525250673
0.198362363	6.653464691	16.525250673
5.385662336	1.388564797	16.525250673
5.385662336	6.653464691	16.525250673
2.480048238	4.127049950	16.844749451
2.480048238	9.391950158	16.844749451
7.667348134	4.127049950	16.844749451
7.667348134	9.391950158	16.844749451
2.738272100	1.466906520	17.239999771
2.738272100	6.731806728	17.239999771
7.925571996	1.466906520	17.239999771
7.925571996	6.731806728	17.239999771
10.001322431	3.645943369	17.924499512
10.001322431	8.910843576	17.924499512
4.814022226	3.645943369	17.924499512
4.814022226	8.910843576	17.924499512
3.000853028	2.325506482	7.596500218
3.000853028	7.590406533	7.596500218
8.188153542	2.325506482	7.596500218
8.188153542	7.590406533	7.596500218
0.150327960	10.314255157	7.894500345
0.150327960	5.049355263	7.894500345

5.337628252	10.314255157	7.894500345
5.337628252	5.049355263	7.894500345
2.601949923	0.226496001	10.204999894
2.601949923	5.491396267	10.204999894
7.789250129	0.226496001	10.204999894
7.789250129	5.491396267	10.204999894
10.020203874	2.858946163	10.642249882
10.020203874	8.123846371	10.642249882
4.832903978	2.858946163	10.642249882
4.832903978	8.123846371	10.642249882
2.163830444	2.433226234	12.867499888
2.163830444	7.698126441	12.867499888
7.351130649	2.433226234	12.867499888
7.351130649	7.698126441	12.867499888
4.394991963	10.300250960	13.316500187
4.394991963	5.035350438	13.316500187
9.582292168	10.300250960	13.316500187
9.582292168	5.035350438	13.316500187
1.685353843	0.270299971	15.544499457
1.685353843	5.535200100	15.544499457
6.872654203	0.270299971	15.544499457
6.872654203	5.535200100	15.544499457
3.929172404	2.876004384	15.996749699
3.929172404	8.140904591	15.996749699
9.116472609	2.876004384	15.996749699
9.116472609	8.140904591	15.996749699
4.127430957	0.131938399	17.645749450
4.127430957	5.396838910	17.645749450
9.314731472	0.131938399	17.645749450
9.314731472	5.396838910	17.645749450
1.299314936	2.757122792	17.719750106
1.299314936	8.022022999	17.719750106
6.486615450	2.757122792	17.719750106
6.486615450	8.022022999	17.719750106

Optimized XYZ position for ZnO(11$\bar{2}$0)/M(100) surface

ZnO(11$\bar{2}$0)/M(100)
1.0

10.5298004150	0.0000000000	0.0000000000
-0.0000185309	10.7049999237	0.0000000000
0.0000000000	0.0000000000	29.5009002686

O	Zr	Zn
72	32	8

Cartesian

0.732446969	3.454717398	9.919088364
5.997346878	3.454717398	9.919088364
0.732437670	8.807217598	9.919088364
5.997337818	8.807217598	9.919088364
1.900101304	0.778467596	9.919382095
7.165001392	0.778467596	9.919382095
1.900092006	6.130967617	9.919382095
7.164992332	6.130967617	9.919382095
3.892649651	3.953142405	11.751093864
9.157549858	3.953142405	11.751093864
3.892640352	9.305642128	11.751093864
9.157540321	9.305642128	11.751093864
4.004796505	1.276785254	11.751093864
9.269697189	1.276785254	11.751093864
4.004787445	6.629285812	11.751093864
9.269687653	6.629285812	11.751093864
1.276209474	1.363174677	12.298925400
6.541110039	1.363174677	12.298925400
1.276200175	6.715674877	12.298925400
6.541100979	6.715674877	12.298925400
1.356231332	4.039424419	12.298925400
6.621130943	4.039424419	12.298925400
1.356222153	9.391924858	12.298925400
6.621121883	9.391924858	12.298925400
4.409030437	4.458525181	14.226809502
9.673931122	4.458525181	14.226809502
4.409020901	9.811025620	14.226809502
9.673921585	9.811025620	14.226809502
3.488309145	1.782275438	14.226809502
8.753209114	1.782275438	14.226809502
3.488299847	7.134775639	14.226809502
8.753199577	7.134775639	14.226809502
0.855857611	2.636427402	14.953120232
6.120757580	2.636427402	14.953120232

0.855848372	7.988927364	14.953120232
6.120748520	7.988927364	14.953120232
1.776578784	5.312677383	14.953120232
7.041479111	5.312677383	14.953120232
1.776569486	10.665177345	14.953120232
7.041469574	10.665177345	14.953120232
3.908656597	3.055635214	16.881006241
9.173556328	3.055635214	16.881006241
3.908647299	8.408135414	16.881006241
9.173547745	8.408135414	16.881006241
3.988687754	0.379385203	16.881006241
9.253587723	0.379385203	16.881006241
3.988678455	5.731885433	16.881006241
9.253579140	5.731885433	16.881006241
1.259784460	0.464597017	17.426181793
6.524684429	0.464597017	17.426181793
1.259775281	5.817096710	17.426181793
6.524675369	5.817096710	17.426181793
1.372659326	3.140846968	17.426181793
6.637559891	3.140846968	17.426181793
1.372650146	8.493347168	17.426181793
6.637550354	8.493347168	17.426181793
4.536021233	3.641519785	19.255533218
9.800920486	3.641519785	19.255533218
4.536011696	8.994020462	19.255533218
9.800911903	8.994020462	19.255533218
3.361215830	0.965376914	19.255237579
8.626115799	0.965376914	19.255237579
3.361206532	6.317876816	19.255237579
8.626107216	6.317876816	19.255237579
2.108901501	3.981938839	20.222867966
7.373802185	3.981938839	20.222867966
2.108892202	9.334438324	20.222867966
7.373792648	9.334438324	20.222867966
0.523223519	1.305688858	20.222867966
5.788123608	1.305688858	20.222867966
0.523214281	6.658188820	20.222867966
5.788114548	6.658188820	20.222867966
0.242281541	5.304755688	10.875211716
5.507182121	5.304755688	10.875211716
0.242272273	10.657256126	10.875211716
5.507172585	10.657256126	10.875211716
2.390470743	2.628612757	10.875211716
7.655371189	2.628612757	10.875211716

2.390461445	7.981112480	10.875211716
7.655362129	7.981112480	10.875211716
2.858936787	5.349395275	13.169496536
8.123836517	5.349395275	13.169496536
2.858927488	10.701895714	13.169496536
8.123827934	10.701895714	13.169496536
5.038399220	2.673145533	13.169496536
10.303299904	2.673145533	13.169496536
5.038390160	8.025646210	13.169496536
10.303290367	8.025646210	13.169496536
0.226488337	4.421807289	16.010433197
5.491388798	4.421807289	16.010433197
0.226479083	9.774307251	16.010433197
5.491379738	9.774307251	16.010433197
2.405951023	1.745664239	16.010433197
7.670851231	1.745664239	16.010433197
2.405941725	7.098164558	16.010433197
7.670841694	7.098164558	16.010433197
2.874522448	4.465911865	18.307373047
8.139422417	4.465911865	18.307373047
2.874513149	9.818411827	18.307373047
8.139412880	9.818411827	18.307373047
5.022711754	1.789661884	18.307373047
10.287611961	1.789661884	18.307373047
5.022702217	7.142161846	18.307373047
10.287602425	7.142161846	18.307373047
2.260534048	2.102997065	20.273902893
7.525434017	2.102997065	20.273902893
2.260524750	7.455497265	20.273902893
7.525424957	7.455497265	20.273902893
0.371588349	4.779247284	20.273902893
5.636488914	4.779247284	20.273902893
0.371579111	10.131747246	20.273902893
5.636479378	10.131747246	20.273902893

References

(1) Huang, S.-D.; Shang, C.; Kang, P.-L.; Liu, Z.-P. Atomic Structure of Boron Resolved Using Machine Learning and Global Sampling. *Chem. Sci.* **2018**, *9* (46), 8644–8655. 10.1039/C8SC03427C.

(2) Huang, S.-D.; Shang, C.; Zhang, X.-J.; Liu, Z.-P. Material Discovery by Combining Stochastic Surface Walking Global Optimization with a Neural Network. *Chem. Sci.* **2017**, *8* (9), 6327–6337. 10.1039/C7SC01459G.

(3) Behler, J.; Parrinello, M. Generalized Neural-Network Representation of High-Dimensional Potential-Energy Surfaces. *Phys. Rev. Lett.* **2007**, *98* (14), 146401. 10.1103/PhysRevLett.98.146401.

(4) Zhang, X.-J.; Shang, C.; Liu, Z.-P. Double-Ended Surface Walking Method for Pathway Building and Transition State Location of Complex Reactions. *J. Chem. Theory Comput.* **2013**, *9* (12), 5745–5753. 10.1021/ct4008475.

(5) Zhang, X.-J.; Shang, C.; Liu, Z.-P. From Atoms to Fullerene: Stochastic Surface Walking Solution for Automated Structure Prediction of Complex Material. *J. Chem. Theory Comput.* **2013**, *9* (7), 3252–3260. 10.1021/ct400238j.

(6) Zhang, X.-J.; Liu, Z.-P. Reaction Sampling and Reactivity Prediction Using the Stochastic Surface Walking Method. *Phys. Chem. Chem. Phys.* **2015**, *17* (4), 2757–2769. 10.1039/C4CP04456H.

(7) Shang, C.; Liu, Z.-P. Stochastic Surface Walking Method for Structure Prediction and Pathway Searching. *J. Chem. Theory Comput.* **2013**, *9* (3), 1838–1845. 10.1021/ct301010b.

(8) Huang, S.-D.; Shang, C.; Kang, P.-L.; Zhang, X.-J.; Liu, Z.-P. LASP: Fast Global Potential Energy Surface Exploration. *WIREs Comput Mol Sci* **2019**, e1415. 10.1002/wcms.1415.

(9) Kresse, G.; Joubert, D. From Ultrasoft Pseudopotentials to the Projector Augmented-Wave Method. *Phys. Rev. B* **1999**, *59* (3), 1758–1775. 10.1103/PhysRevB.59.1758.

(10) Blöchl, P. E. Projector Augmented-Wave Method. *Phys. Rev. B* **1994**, *50* (24), 17953–17979. 10.1103/PhysRevB.50.17953.

(11) Perdew, J. P.; Burke, K.; Ernzerhof, M. Generalized Gradient Approximation Made Simple. *PHYSICAL REVIEW LETTERS* **1996**, *77* (18), 4. 10.1103/PhysRevLett.77.3865.

(12) Grimme, S.; Ehrlich, S.; Goerigk, L. Effect of the Damping Function in Dispersion Corrected Density Functional Theory. *J. Comput. Chem.* **2011**, *32* (7), 1456–1465. 10.1002/jcc.21759.

(13) Grimme, S.; Antony, J.; Ehrlich, S.; Krieg, H. A Consistent and Accurate Ab Initio Parametrization of Density Functional Dispersion Correction (DFT-D) for the 94 Elements H-Pu. *J. Chem. Phys.* 20. 10.1063/1.3382344.

(14) Liu, X.; Zhou, W.; Yang, Y.; Cheng, K.; Kang, J.; Zhang, L.; Zhang, G.; Min, X.; Zhang, Q.; Wang, Y. Design of Efficient Bifunctional Catalysts for Direct Conversion of Syngas into Lower Olefins *via* Methanol/Dimethyl Ether Intermediates. *Chem. Sci.* **2018**, *9* (20), 4708–4718. 10.1039/C8SC01597J.